Composite Structures 275 (2021) 114488

Contents lists available at ScienceDirect

Composite Structures

journal homepage: www.elsevier.com/locate/compstruct

Hierarchical homogenization and experimental evaluation of functionally graded materials manufactured by the fused filament fabrication process

Seymur Hasanov [a], Ankit Gupta [a], Frank Alifui-Segbaya [b], Ismail Fidan [c,*]

[a] Department of Mechanical Engineering, Tennessee Tech University, Cookeville, TN 38505, USA
[b] School of Medicine and Dentistry, Gold Coast Campus, Griffith University, Southport, QLD 4222, Australia
[c] Department of Manufacturing and Engineering Technology, Tennessee Tech University, Cookeville, TN 38505, USA

ARTICLE INFO

Keywords:
Fused filament fabrication
Functionally graded materials
Fiber reinforced composites
Homogenization
Finite element method

ABSTRACT

This research study investigates the numerical and experimental characterization of Functionally Graded Materials (FGMs) fabricated by the fused filament fabrication (FFF) process. To design and fabricate FGMs, the gradient-based digital structures were designed using the voxelization method and manufactured with flat and on edge printing orientations. The direct and gradual transition patterns were fabricated, and tensile test method was used to characterize the interface strength. The results indicated that the gradual change in fiber reinforcement reduced the stress concentrations at the interface zone and increased the strength of neat Acrylonitrile Butadiene Styrene (ABS) properties. The homogenization approach was applied along with the finite element method to predict the effective material properties of FFF-made FGMs. It was found that the homogenized values were close to the experimental test results with around 5 % error for flat-oriented parts. Overall, this research work presents an important step toward enabling the effective design and analysis of composite structures using an experimental characterization and computational methodology.

1. Introduction

Additive Manufacturing (AM) is a layer-by-layer manufacturing process used to fabricate three-dimensional (3D) objects directly from computer aided design (CAD) model data [1]. AM has several advantages in that it produces lighter products; has less material waste and fewer assembly steps, lower lead time, and no added costs; and can produce customized complex parts [1,2]. However, most AM systems are limited in terms of single material deposition, leading to a performance entirely dependent upon geometry. Among the various AM methods, fused filament fabrication (FFF) is one of the most popular, being extensively implemented to produce polymer and composite structures [2,3]. Novel AM systems have been adapted to deposit multiple materials in a single manufacturing process, allowing deliberate placement of each material. Recently, AM methods have enabled the fabrication of multi-material complex geometries with site-specific properties [4].

With the advancement of the FFF process, multi-material structures can be 3D printed with the gradient interface regions using a single extruder machine, which allows for the functional multi-material composite parts to be produced directly from the design stage [5]. The multi-material FFF process is key to fabricating advanced components using a variety of materials available in the market. The ability to produce multiple materials in a single fabrication process makes the blending of various similar and dissimilar materials possible. In the conventional multi-material AM process, joining two materials is limited to discrete interface regions, which create high-stress concentration areas and potential failure zones. Hence, functionally graded materials (FGMs) could be deposited at a specific area of the component with an enhanced interface region to locally improve the overall thermo-mechanical performance of the final part [6,7]. FGM is an advanced engineering material, which is characterized by the variation in composition and structure over volume, resulting in corresponding changes in the properties of the material [7]. In recent years, FGMs have experienced considerable attention in the materials science and engineering society, which has led to the development of other manufacturing methods. FGMs are of great interest to a larger range of industrial sectors and applications including the aerospace, automobile, energy-absorbing structures, optoelectronic devices, and biomedical implant industries [8]. Today, various AM methods can fabricate FGMs using unique manufacturing techniques [9–13].

* Corresponding author.
E-mail address: ifidan@tntech.edu (I. Fidan).

https://doi.org/10.1016/j.compstruct.2021.114488
Received 26 May 2021; Revised 16 July 2021; Accepted 30 July 2021
Available online 3 August 2021

Fiber-reinforced composites fabricated by AM processes have grained tremendous attention from the aerospace, automobile and medical industries due to the advantages of enabling the production of complex, lightweight, and high-performance composite materials [2,14–16]. Mechanical properties of FFF-made fiber-reinforced composites have been extensively investigated. Fabrication of composite FGMs with the FFF method is however new and hence the evaluation of microstructure, composition, mechanical properties, and computational modeling of these structures are pertinent.

One of the goals of the current work is to characterize the strength of material interfaces, for example, the one with *neat* material property and the other one reinforced with short carbon fibers. Conventional manufacturing techniques cannot allow internal features of the composites to be customized with integrated functionalities. In addition, the volume, amount, shape, and location of reinforcement in the matrix material can be accurately controlled to allow each material to be deliberately placed in a single structure to achieve the desired mechanical property for a specific application. To this end, understanding of mechanical properties and computational modeling of FGMs with fiber reinforcement is crucial. In addition, microstructural analysis is performed to investigate the internal feature of the composite materials. Micrography of printed composites allows the effect of fiber reinforcement, fiber breakage, and fiber orientation on the mechanical properties of FGMs to be studied.

Numerical simulation of composite structures is challenging due to the differences in involved length scales. While the finite element method could be used to simulate the structural mechanics of this system (resolve all length scales), it requires a lot of computational time. Homogenization is the standard approach for eliminating this problem of scale in finite element analysis (FEA) for composite materials. With homogenized material data, structures only need to be simulated at the macroscopic scale, making composite simulation significantly less expensive computationally.

To computationally model the fiber-reinforced composites, the multiscale modeling method has been utilized by researchers [17–19]. Multiscale modeling is a hierarchical computational process that allows material properties of fiber-reinforced FFF made FGMs to be predicted [20,21]. This method would eliminate the need for experimental evaluations to predict the effective material properties that can later be used for finite element simulations of composite structures. However, design and analysis of FFF-made composite materials are key challenges due to the anisotropy present in the microstructure of the fabricated parts [22,23]. Since the 3D-printed composite parts have directional properties, and their material behavior is highly dependent on the process-induced microstructure (e.g., the volume fraction of fiber and voids and fiber orientation) [24], it is essential to consider these effects in computational modeling. An FFF-made FGM composite consists of several involved scales:

- Microscale: the domain of short carbon fiber reinforced ABS
- Mesoscale: the shape of the bead and interbead voids
- Macroscale: Specimen geometry with gradient transition between materials

Fig. 1 depicts the three-scale homogenization framework applied in this research.

Recently, Gupta et al. investigated the effect of process parameters of short-fiber reinforced polycarbonate polymer matrix composites fabricated by the FFF process. The authors found that the fiber behavior inside the composite influenced the mechanical performance of the final parts. In their study, it was found that printing direction and fiber reinforcement percentage were the most influential parameters [25]. Several research studies have addressed the homogenization and lamination theory of the mesoscale geometry of FFF-made *neat* parts using the homogenization approach [23,26–29]. Nasirov et al. performed multiscale modeling of FFF-made fiber-reinforced composite parts using an asymptotic homogenization method by involving three-scale hierarchy. A microscale representative volume element (RVE) with different fiber volume fractions and orientations (aligned and random) was successfully generated. Material property obtained from the microscale was then incorporated into the mesoscale RVE to employ the homogenization method. It was concluded that the predicted Young's modulus that considers random fiber orientation with an actual RVE microstructure is sufficiently precise compared to the experimental test results [23,30]. In another research study by Somireddy et al., a homogenization method was applied to computationally model the fiber-reinforced ABS composites. It was found that the elastic moduli obtained from the presented method precisely characterized the mechanical behavior of printed parts [28]. Babu et al. performed the RVE generation procedure for fiber-reinforced microstructures by considering the fiber orientations derived from the fiber-infused microstructure with different fiber orientations [31]. Another research study investigated the effective material properties of the tungsten-infused, metal-matrix composite derived from the microstructural information using the homogenization method. It was concluded that errors between the proposed method and the experimental results showed less than 10.5 % error [32]. Additionally, Cuan-Urquizo et al. used the FEA along with micromechanical methods to predict the mechanical behavior of 3D printed parts for different infill densities [33]. In their study, the errors found between micromechanics and FEA simulations were negligible. Moumen et al. reviewed computational modeling of additively manufactured composites [34]. Wang et al. performed a research study to investigate the prediction of mechanical properties of short carbon-fiber reinforced composite parts fabricated by the AM method [35]. The predicted fiber orientation was used to estimate its effect on the mechanical properties; however, the research study only focused on the numerical modeling and simulation of fiber-reinforced composites without further validation of the results using experimental or other methods.

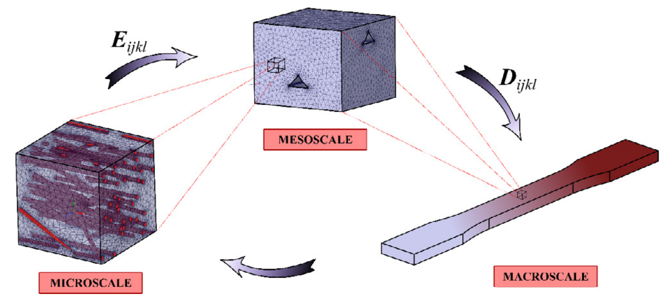

Fig. 1. Three-scale homogenization framework.

Besides the mentioned research studies regarding the FFF-made composites, characterizing the multi-material interfaces is an important step in manufacturing FGMs with enhanced boundary quality. The abrupt changes in mechanical behavior at the interfaces between two dissimilar or similar products with different thermo-mechanical properties can lead to mechanical failure. As compared to conventional multi-material composites, FGMs could be much more robust due to their gradient transitions, which can reduce the mechanical stress concentrations, hence preventing delamination at crack-sensitive areas and improving the durability of loadbearing components [8]. Previous research studies focused on the influencing factors of the AM technique on the interface strength of multi-material structures. Lopes et al. [36] studied the effect of the bonding mechanism on the interface performance of printed multi-material parts. In their study, only discrete material interfaces with different material combinations have been investigated. It was revealed that the chemical aspect of the material affinity must be considered to understand the physical aspect. Hasanov et al. investigated the variations of interface properties of dissimilar polymer material combinations using the tensile testing method [5]. Different interface patterns were designed using the voxelization method and fabricated by the multi-material FFF process. It was found that gradient transition of interface yielded higher strength and stiffness values than interlock and direct transitions of PC and ABS materials. Brackett et al. investigated the material transition behavior from *neat* ABS to short carbon fiber (SCF) reinforced ABS using a Big Area Additive Manufacturing (BAAM) blended extrusion process [37]. It was found that the transition between materials is directionally dependent, with ABS to CF/ABS having a change length of 3.5 m compared to 3.2 m for CF/ABS to ABS. Conventional sandwich panel designs that are fabricated by the AM processes experience structural weak points and fracture at the material interface. Vu et al. investigated the effect of print orientation on interface integrity of the multi-material jetting AM process [38]. It was found that aligning the interface transition perpendicular to the printing direction increased the fracture resistance. Overall, it can be concluded that a limited number of studies in the literature have investigated the mechanical properties of fiber-reinforced FGMs fabricated by the FFF process using numerical and experimental methods.

In the present work, design, fabrication, and numerical and experimental characterization of composite FGMs have been studied. Fabrication of composite FGMs using the FFF process allows multi-material structures with locally improved strength and stiffness properties to be obtained. Mechanical characterization of FGM parts performed using the tensile test specimens fabricated with flat *(XY)* and on-edge *(XZ)* printing plane orientations. Microstructural description was used to evaluate the fiber orientation and length distribution in the printed parts. Hierarchical computational models were applied to the material modeling of FFF-made FGM composites. The properties of neat ABS and SCF were employed to determine the material behavior of microscale domain of composite. Then mesoscale material properties of ABS alone or SCF reinforced ABS were computed by considering interbead voids which was inherited during layer deposition process. Material behavior of fabricated FGM composite was then computed by applying various gradient functions at macroscale to determine gradual change of material properties throughout structure. Developed model was used to estimate material behavior of different interface patterns and predicted values were compared with the experimental test results to validate the proposed approach. In addition, concentrations of ABS and CF/ABS composites were fabricated and mechanically tested. This is conducted to understand the material behavior of the heterogeneous composite at certain volume fraction of FGM material. Homogenized material properties of heterogeneous composite were then validated using experimental test results. Finally, results and further work regarding the development of computational design methodology for effective design and analysis of FFF-made composites are discussed.

2. Materials and methods

2.1. Design of digital structures

To represent material distribution on the CAD data, a voxel (the unit for volumetric pixel) was used to design FGM specimens. A voxel is the form of a rectangular pixel that represents a 2D image as a bitmap, which is the smallest unit in a 3D volume data obtaining a logical value, with one defining a solid space and zero defining a void space. Mesh-based CAD data such as the standard tessellation language (STL) represents only geometrical information. However, the voxel-based design method can accommodate heterogeneous material information, which can be used to design graded components. Voxels are closer to determining the real characteristics than the traditional STL approach [39,40]. The workflow of the voxel-based approach is given in Fig. 2.

Several research studies performed the voxel-based representation schemes to fabricate FGM structures through AM methods. Ituarte et al. used voxel-based methodology to design and fabricate FGMs based on digital materials [13]. The mechanical behavior of fabricated parts using a material jetting technique was defined by the combined effect of mechanical properties of the base materials used at the voxel-scale (~90 μm). Doubrovski et al. presented a bitmap printing method and digital workflow using a multi-material high resolution AM process. They designed the material composition based on the predefined voxel resolution to print objects with locally varying material properties, aiming to satisfy the design objective [41]. In this research, the voxelization method was applied to the macroscale representation of the FGMs.

One of the objectives of this study is to characterize the interface of multi-material components. Hence, different interface transition patterns such as direct transition and continuous gradient transitions were designed using Voxelizer software (ZMorph, Poland) and tested using the mechanical method. To understand the effect of gradient length at the interface region, 5%, 10%, 30%, and 100% length of the overall test specimen was determined as the FGM transition. The material properties of 3D printed composites differ from those of the materials used to fabricate them and create anisotropy in the final part. Therefore, *XY* and *XZ* printing plane orientations were used to manufacture the FGM specimens. Infill orientation was defined as 0/90 layup and fixed for all specimens. Fig. 3 shows the designed interface patterns along with their defined functions.

2.2. Experimental setup

A single nozzle multi-material 3D printer was used to manufacture the FGM specimens with different printing orientations. The process description of the multi-material FFF technique is presented in Fig. 4. The design capability of the FFF process allows two filaments to be fed directly to the same melting zone and extruded simultaneously based on an adjustable ratio of materials.

In this research study, ABS and SCF reinforced ABS were used to fabricate FGM composites. Processing parameters employed for the printing process and material data are shown in Table 1 [17,25,42].

Mechanical testing was performed using an Instron 5582 UTM tensile machine at room temperature. The procedure was conducted in accordance with ASTM D638 “Standard Test Method for Tensile Properties of Plastic” [43]. Test specimens with a 50 mm gauge length were fabricated in two printing directions such as *XY* and *XZ* with a 0/90 layup orientation and tested with a strain rate of 5 mm/min. In addition, direct and FGM with 5%, 10%, 30%, and 100% transition patterns of ABS and carbon fiber reinforced ABS (CF/ABS) were used to characterize the interface strength.

2.3. Computational method

The homogenization theory developed from studies of partial differential equations and two explicit assumptions are considered. One of the assumptions is that fields vary on multiple spatial scales due to the existence of a microstructure. Second, it is assumed that the microstructure is locally periodic [44]. Homogenization is an accurate approach in performing an FEA on the microscale structure of the material and is the approach implemented in this research. As the homogenization process starts modeling with RVE, the creation of a simplified geometry, as well as the definition of material properties of the constituent materials, is required. Subsequently, the geometry is meshed for FEA. The RVE is then exposed to several macroscopic load cases, and its response is computed, resulting in the homogenized material data [45].In this context, defining the properties of the base materials and the RVE is an essential step toward homogenization. An RVE is defined as the smallest periodic volume element of a material with an accurate statistical representation of the typical material properties used in a macroscale model. In this study, an RVE is taken from the microstructure of the FFF-made parts to perform numerical homogenization. RVE is considered through scales from micro to meso

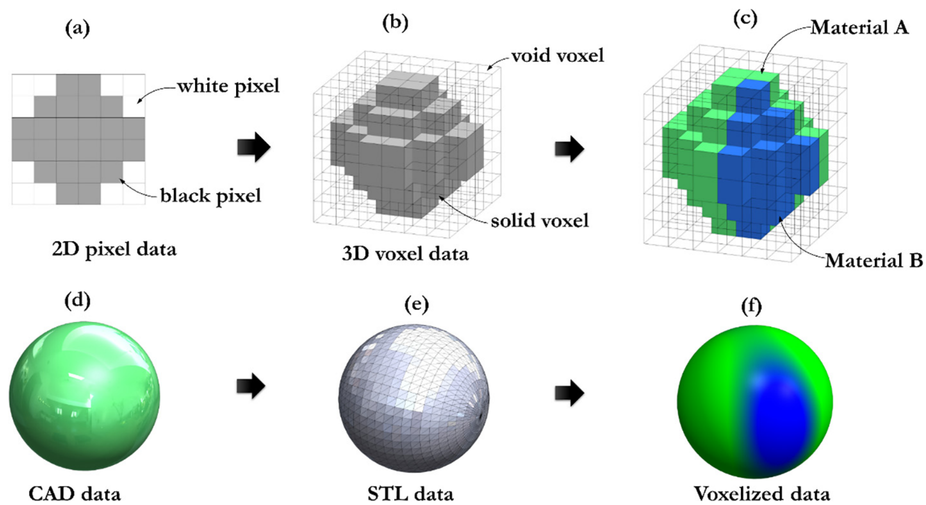

Fig. 2. Voxel-based workflow representing FGM objects, (a) 2D pixel image; (b) 3D voxel model; (c) defined materials for each voxel; (d) CAD model data; (e) STL data containing only geometrical information; (f) voxelated data generated from STL model, which contains two different material phases.

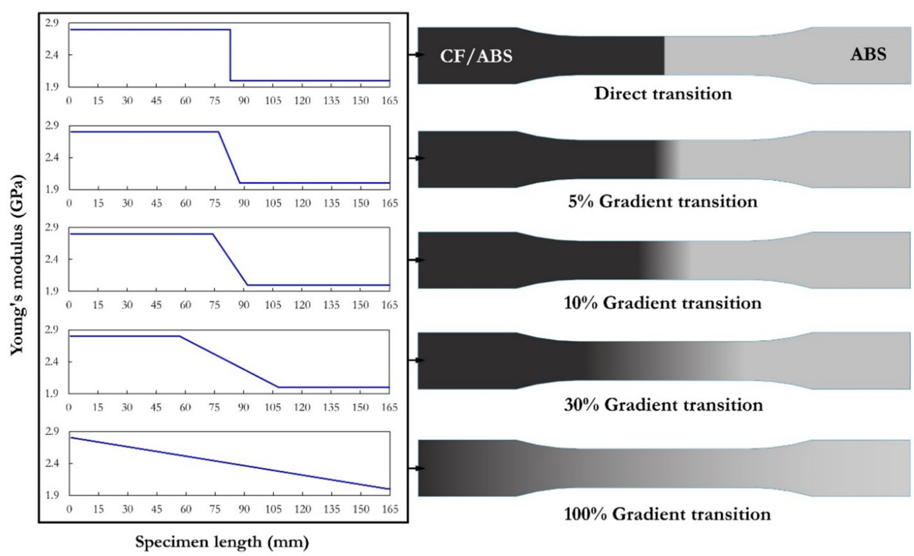

Fig. 3. Designed interface patterns, (a) material transition functions, (b) tensile test specimens with various transitions from CF/ABS to neat ABS material.

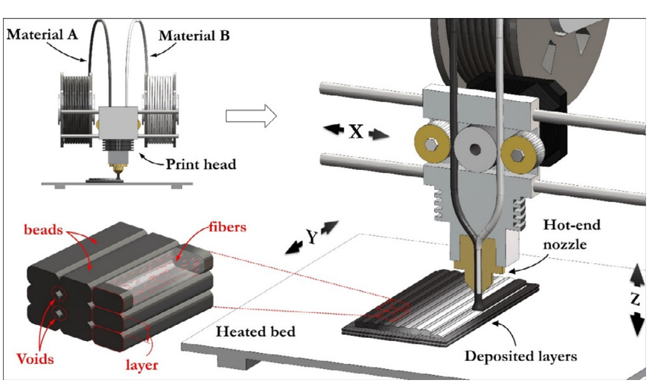

Fig. 4. Process description of the multi-material fused filament fabrication process.

and from meso to macro. Microscale RVE consists of the short fiber reinforcement and the matrix (ABS) material. Mesoscale RVE consists of the deposited beads and layers, which create voids during the fabrication process. Here, the homogenization approach determines the effective constitutive matrix of the fibers infused into the matrix and layer of the FFF-made composite parts using the data of the microstructural and mesostructured information. Homogenization methods have been available for a long time, and detailed information can be found in the literature [28,44,46,47].

The RVE is considered a macroscopically homogeneous orthotropic material, and the stresses and strains are the local fields at a point in the RVE. At a macroscopic level, average stress and strain fields are calculated by averaging the local stresses and strains over the volume of RVE, respectively. The average stress and strain field is given below:

$$\overline{\sigma}_{ij} = \frac{1}{|\Theta|}\int_{\Theta}\sigma_{ij}(x,y,z)d\Theta, \overline{\varepsilon}_{ij} = \frac{1}{|\Theta|}\int_{\Theta}\varepsilon_{ij}(x,y,z)d\Theta \quad (1)$$

whereΘ indicates the volume of RVE, $\overline{\sigma}_{ij}$, $\overline{\varepsilon}_{ij}$ are the average stress and strains, $\sigma_{ij}(x,y,z)$, and $\varepsilon_{ij}(x,y,z)$ are the local stress and strain of the RVE defined in the local coordinate system of x, y, and z. The relationship between the average fields of SCF and the matrix in an RVE is as follows:

Table 1
Printing process parameters and material properties.

Process parameters			Base material properties	
			ABS	SCF
Nozzle temperature (°C)	245	Melting point (°C)	245	–
Bed temperature (°C)	100	Density (g/cm^3)	1.12	1.81
Infill density (%)	100	Tensile strength (MPa)	44.1	4137
Infill pattern	0/90	Elastic modulus (GPa)	2.39	242
Layer height (mm)	0.18	Glass transition temperature (°C)	101	–
Printing speed (mm/s)	20	Flexural strength (MPa)	59	–

$$\bar{\varepsilon}_{ij} = v_f\bar{\varepsilon}^f_{ij} + v_m\bar{\varepsilon}^m_{ij}, \bar{\sigma}_{ij} = v_f\bar{\sigma}^f_{ij} + v_m\bar{\sigma}^m_{ij} \tag{2}$$

In Eq. (2), f denotes SCF and m denotes matrix material, respectively.

Once the homogenization procedure is completed, stress and strain tensors for each RVE will be available to compute equivalent material properties. The relationship between $\bar{\sigma}$ and $\bar{\varepsilon}$ is:

$$\{\bar{\sigma}\} = [\boldsymbol{C}]\{\bar{\varepsilon}\} \tag{3}$$

where C is the effective stiffness tensor of the RVE.

The constitutive matrix is obtained by applying six different strains of ε^0_{ij} to the RVE domain, enforcing the displacement field on the boundary surface of the RVE. When the RVE is subjected to various boundary conditions, the coefficients of the effective stiffness tensor $\boldsymbol{C}$ are computed by solving six boundary value problems (BVP). For each of the BVP, only one strain of ε^0_{ij} value is different from zero. It means that the finite element (FE) model of the RVE being subjected to a unit strain is prepared for six different strain load cases. More detailed discussion regarding the theory can be found in [45]. Then, the results lead to computing average local stress and strain fields, and finally effective stiffness tensor.

Overall, a three-scale homogenization framework is given in Fig. 5 and starts with the approximation of fiber orientation and length distribution using the microstructural description.

Since the fiber angle orientation significantly affects the composite material property, orientation tensor was then computed using the fiber angle distribution. The microscale RVE was modeled using the finite element (FE) method. Homogenization along with the FE modeling was conducted in Ansys Material Designer (ANSYS Inc., USA). RVE was modeled with smaller finite elements to avoid the mesh dependency. Homogenized microscale material property was then employed to find the mesoscale CF/ABS material property. Mesoscale RVE was modeled in both cases of neat, printed ABS and CF/ABS materials.

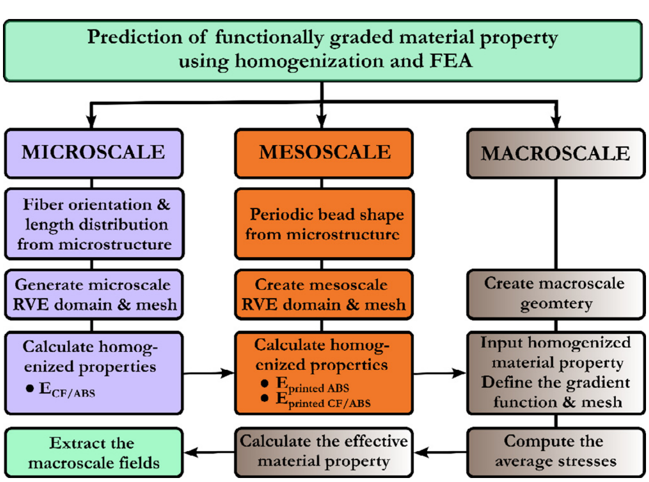

Fig. 5. Three-scale homogenization framework for calculating effective material properties of FGM composites.

After homogenizing printed material property for the ABS and CF/ABS case, the base material properties were then incorporated into the FE implementation of a tensile test specimen with predefined gradient functions. The following steps involve the averaging of stresses throughout the area of the specimen and finding the effective material property for FGM.

2.4. Microscale and mesoscale RVE generation

Various RVE generation algorithms for the composite microstructure are reported in literature. The main limitation of most RVE generation algorithms is the constraint of fiber concentration percentage in the matrix material with a given aspect ratio (AR). Fiber AR is dependent on the diameter and the length of the fiber, which is the ratio of fiber length to fiber diameter. Nominal fiber diameter and the approximate fiber length have been obtained from the microstructural images of the deposited layers. Fiber length can be different or broken after the extrusion process due to fiber-to-fiber interaction and contact with extruder screw threads. Therefore, microscopic images are used to estimate fiber length distribution in the deposited composite layers.

In the present study, digital analysis of fiber orientation using image processing software is presented to compute approximate fiber orientation tensor. Types of fibers and their orientation in a polymer matrix are important factors determining the properties of produced material [2,17,48,49]. Therefore, image analysis is used to estimate the fiber angle and length distribution in the matrix material. The adopted AR of fibers is found to be 20 using microscopic measurements. Fig. 6 shows the RVE shape obtained from microstructural description.

ImageJ software was utilized to analyze the orientation of the fibers [50]. This program is widely used in the scientific community to analyze the microstructural images. A series of microstructural images were taken using the optical microscope to investigate the fiber orientation and length distribution inside the matrix material. Fig. 7 shows one of the sample images used to calculate the approximate fiber orientation with respect to the printing direction. Approximate fiber angle orientations were less than about 5° with respect to the printing direction. It should be noted that only clearly shown fibers are measured on the cross-section of the microstructure. In addition, approximate fiber length was determined to be around 150 μm based on image analysis of the microstructure.

Thermogravimetric analysis (TGA) was performed to identify the fiber volume fraction in the printed parts. It was found that weight fraction (W_f) of fibers inside the printed part was nearly 6.889%. The relationship between volume and weight fraction of the fiber and matrix can be calculated using Eq. (4):

$$W_f = \frac{\rho_f V_f}{\rho_f V_f + \rho_m (1 - V_f)} \tag{4}$$

where the W_f indicates the weight fraction of the fiber, ρ_f and ρ_m are the densities of fiber and matrix respectively, and V_f is the volume fraction of the fiber. Since the weight fraction of the fiber was found using the TGA method, the volume fraction of the fibers can easily be calcu-

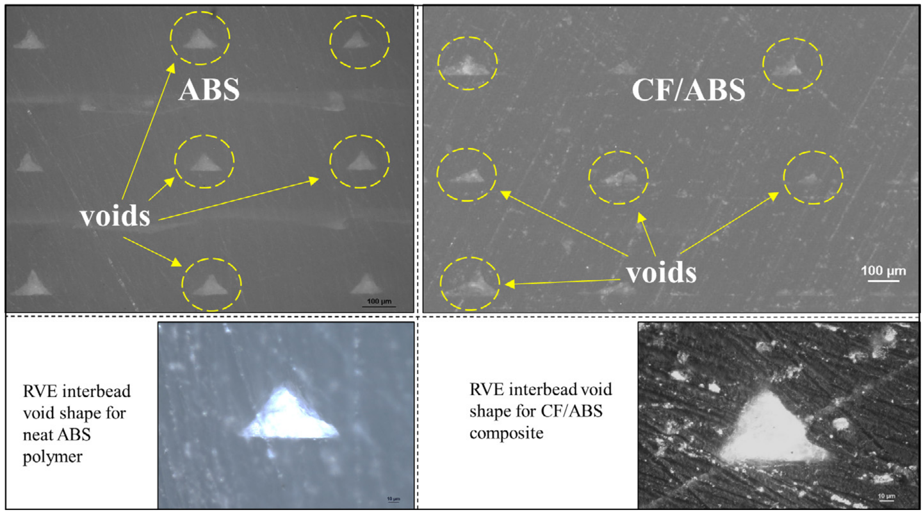

Fig. 6. No text of specified style in document.. Microstructure of neat ABS and CF/ABS parts fabricated by the FFF process.

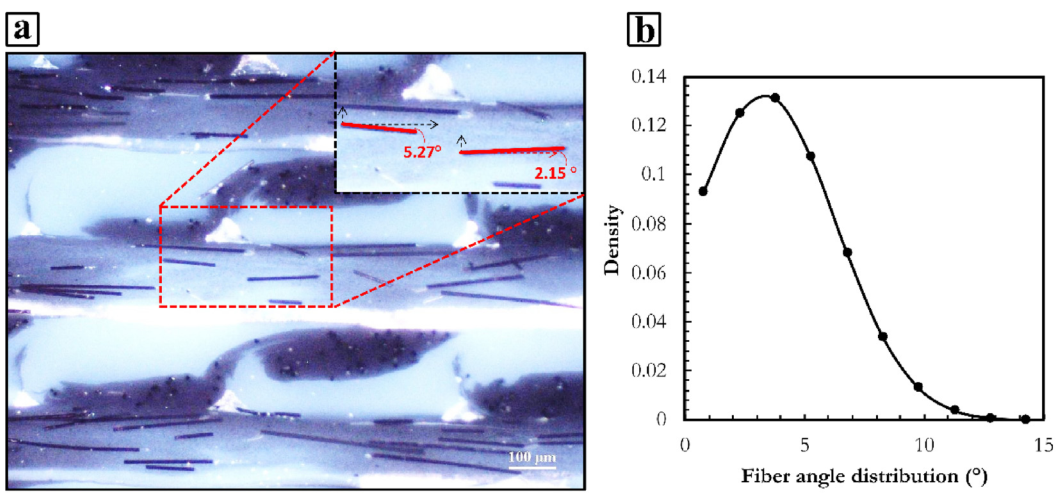

Fig. 7. Cross-sectional view of microstructure of fiber reinforced FGM sample that is used to estimate the fiber orientation distribution with respect to the printing direction, (a) micrography of the FGM part, (b) fiber angle distribution.

lated. The volume fraction of fiber content (V_f) in this research study was found to be approximately 4.71 %.

After finding the fiber volume fraction and orientation tensor of the fabricated CF/ABS composite, the RVE of the microscale was generated. Fig. 8 shows the microstructure of the mesoscale RVE where the periodic voids were observed. These voids influence the material property after the 3D printing process. Therefore, due to their periodic nature, they are considered during the homogenization process at mesoscale.

Fig. 8 also indicates the implementation of finite elements on the micro and mesoscale RVE of CF/ABS composite material before the homogenization process. Since the RVE layup has a 0/90 orientation, the fiber orientation was also considered separately in 0- and 90-degree directions.

2.5. FE implementation on macroscale

FEA was performed to obtain the effective macroscale material property and to validate the proposed design approach with the experimental results. The linear gradient function was employed to change the material properties. The equation below shows the gradient function used to compute Young's modulus and Poisson's ratio:

$$\boldsymbol{M}(x_q, y_q) = \frac{(\boldsymbol{M}_{CF/ABS} - \boldsymbol{M}_{ABS}) \cdot f(x_q, y_q)}{\Delta L} + \boldsymbol{M}_{ABS} \tag{5}$$

where $\boldsymbol{M}(x, y)$ is the material property that varies linearly along the x or y axis; $\boldsymbol{M}_{ABS}$ and $\boldsymbol{M}_{CF/ABS}$ are the mesoscale material property of ABS and CF/ABS, respectively; ΔL is the difference between two coordinate points where the gradation occurs; $f(x_q, y_q)$ indicates the quadrature points of each element that vary linearly along the x or y axis.

Material properties such as Young's modulus $\boldsymbol{E}(x, y)$ and Poisson's ratio $\nu(x, y)$ were evaluated at the quadrature points of each element. The FE method for graded elements using an isoparametric formulation was implemented [51]. The average stress (σ_{avg}) was computed by integrating stresses (σ_{xx}) along the load direction and dividing them by the overall area of the tensile specimen [52]. Then, the effective Young's modulus ($\mathbb{E}$) was computed by dividing the average stress (σ_{avg}) by strain value (ε_{xx}) at the far end of the specimen:

$$\mathbb{E} = \frac{\sigma_{avg}}{\varepsilon_{xx}} \tag{6}$$

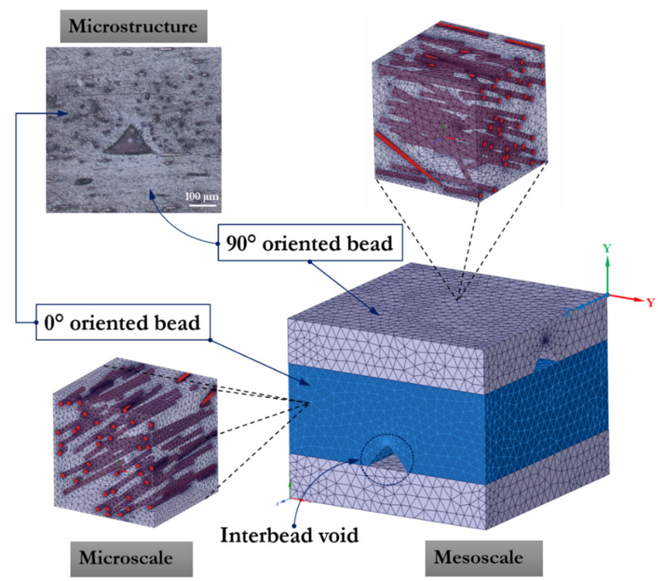

Fig. 8. Microscale and mesoscale RVE models meshed using finite elements.

3. Results and discussion

3.1. Microstructural analysis

Microstructural analysis was performed to investigate the internal morphology of FFF-made FGM composite materials. A static mixer was inserted inside the hot-end nozzle to help in mixing the polymers. Micrography of these materials was also evaluated to understand the effect of the static mixer on the blending of the materials. Fig. 9 shows the cross-section of the material fabricated in a 0/90 layup orientation.

It is evident from the microstructure that fibers are mainly oriented in the printing direction. ABS and CF/ABS regions are shown in the microstructure with the interbead voids, which are created during the deposition of the layers. Although the static mixer was added inside the nozzle, materials did not properly mix as seen from the microstructure. Since the matrix materials are the same for ABS and CF/ABS, the formation of material phases may create good adhesion, which could help to prevent structural failures such as the delamination of layers. The addition of fiber reinforcement into the ABS matrix enhances its mechanical properties. Changing the volume fractions of SCF throughout the part may influence the mechanical properties as well. In the microstructual image, fibers are uniformly distributed inside the CF/ABS matrix, which eventually helps to enhance the material property of the final composite material.

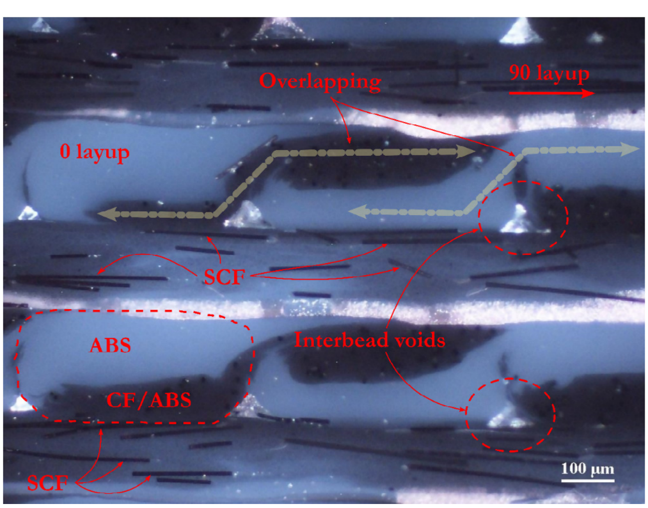

Fig. 9. Microstructural image of FGM sample shows the ABS and CF/ABS material phase.

The goal of fabricating FGM is to observe the bonding strength of multi-material parts at the transition areas and to improve the mechanical performance using appropriate FGM transitions. Poor interface affinity results in weakening of the bonds and affects the overall material performance. Based on microstructural analysis, manufacturing of multi-material components could strengthen the interface affinity by gradually changing the material distribution.

3.2. Analysis of tensile properties

It is crucial to understand the mechanical performance of multi-material components with a gradual interface transition. Tensile test specimens were fabricated with neat ABS, FGMs, and CF/ABS. It should be noted that the FGM here has a linear transition in the Z direction. Fig. 10 indicates the variation of material properties with respect to different printing plane orientations, e.g., *XY* and *XZ*. As shown, the material property changes based on the addition of fiber reinforcement.

FGM parts fabricated on the *XY* plane show enhanced strength and stiffness as compared to neat ABS material. Material property varies linearly and is expected between ABS and CF/ABS. However, specimens manufactured on the *XZ* plane yielded poor tensile behavior in all tested samples. Testing FFF-made specimens perpendicular to the printing direction indicates a weak response because of limited adhesion between the layers that is shown in several studies [5,17,25,53]. FGM tensile test results on the *XZ* plane is around 13–15 MPa, which is lower than *neat* ABS and CF/ABS testing results. Here, the lower response occurred in the *XZ* case because of the applied transverse load with respect to the fiber orientations. In addition, fibers in the second phase may create micro-stresses between the matrix-fiber interface as well which can create extra complications during mechanical load. In this condition, the tensile load is not uniformly distributed from the fibers to the matrix. The stress concentration acts more on the end of the fibers and usually propagates at the matrix-fiber interface, resulting in premature failure or matrix cracking. However, the tensile strength of the CF/ABS material yielded better results than the FGM sample due to the uniform distribution of fibers throughout the specimen.

3.3. Interface strength evaluation

Multi-material components fabricated by the FFF process may have critical interface issues, depending on the adhesion of the layers between two materials. FGM can effectively overcome the interface problems especially between similar and dissimilar materials. A similar material interface could have several issues. For example, changing from one material property at sharp interfaces could result in high stress concentrators at the joint of these materials and could increase the chance of interface failure. Even in connecting two incompatible materials, Udupa et al. [7] and Hasanov et al. [5] argued that FGMs could act as an interfacial layer to enhance the bond strength. Therefore, FGM plays a vital role to fabricate components with better interfacial strength and prevent them from unexpected failures. Here, the custom-made specimen was fabricated to characterize the interface strength between the ABS and CF/ABS materials. Interface characterization was performed between dissimilar materials such as ABS and PC in the previous work [4].

Fig. 11 shows the tensile strength and modulus result of various interface design patterns such as direct, FGM 5%, FGM 10%, FGM 30%, and FGM 100%. FGM specimens were fabricated with different gradient transition length. As shown in the following graph, transition

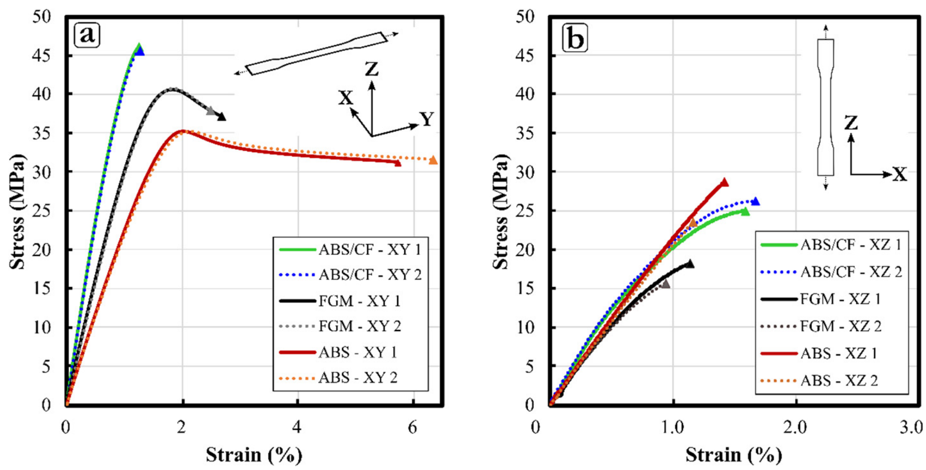

Fig. 10. Stress and strain graph of ABS, CF/ABS and FGM composites fabricated on XY and XZ plane.

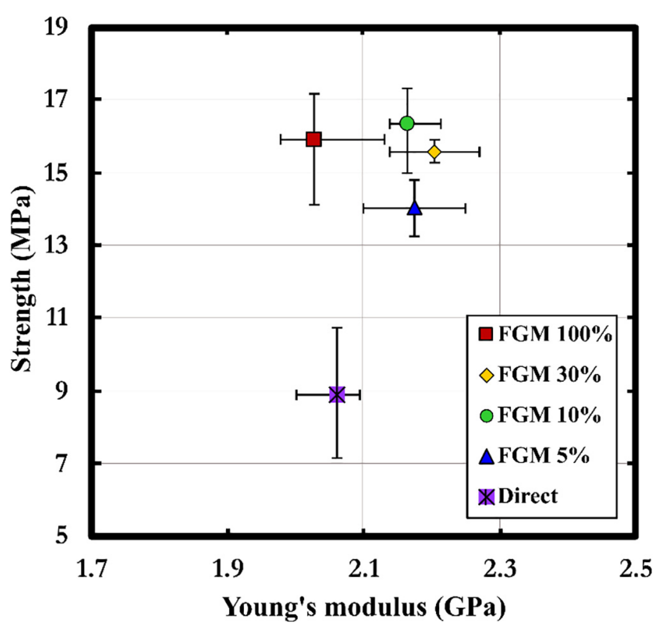

Fig. 11. Variation of strength and Young's moduli of various interface design patterns.

length affects the strength of the interface of the specimens that are fabricated and tested on the *XZ* orientation.

The longer the gradient transition length, the lesser the material abrupt property changes and reduces the stress concentrations between the materials. Although the matrix materials are the same, difference exists in material properties between ABS and CF/ABS materials. The strength of the direct interface is considerably lower than those with gradual transitions, but close to a full FGM transition length in terms of tensile modulus. The FGM of 5% has a slight advantage over the full FGM transition with a stiffer response. The strength and modulus of 10% and 30% FGM transition length are very close to each other (around 15–17 MPa of tensile strength and 2.2 GPa Young's modulus) and indicate a significantly higher interface strength than a direct transition pattern. Results show that although the matrix material is the same, the sharp transition of material properties increased the stress concentrations which also reduced the strength and stiffness of the part. The gradual change of material properties increased the strength by approximately 58% and stiffness by 6% for FGM 5% compared to sharp transition. FGM 10% showed 84% higher strength and 5% stiffer response than direct transition. The length of the gradient transition was also compared between the FGM designs. FGM 10% showed 17% higher tensile strength than FGM 5% due to the increase in gradient transition length. The comparison between FGM 30% and direct transition showed 75% difference in tensile strength as shown in Fig. 12.

It can be seen from Fig. 10 that the strength of FGM 30% dropped by 7% compared to FGM 10%. The highlighted area on the FGM 30% specimen shows the stress concentration zones that led to a drop in tensile strength and hence the gradual change in materials should be considered inside the gauge area.

The difference in material behavior of the specimens could be due to a variety of factors such as poor affinity between layers (when the load is applied transversely to the printing orientation), staircase effect, and the effect of part vibration during the *XZ* printing orientation. Fabricating the specimens with lower layer heights could increase the surface quality and reduce the outer roughness of the specimens fabricated on the *XZ* plane. The higher layer heights increase the chance of crack propagation between layers. However, fabricating specimens with lower layer heights increases printing time significantly and therefore is considered for future work.

Overall, direct transition interfaces fabricated by the FFF process are considered critical and weak joint regions in terms of bond strength. With the advantage of a gradient transition, the bonding strength at the interface could be enhanced to reduce stress concentrations at the multi-material interfaces.

3.4. Homogenization results

Microstructural samples showed that there were fibers inside the matrix and periodic voids between adjacent beads and layers of FFF-made parts. Table 2 shows the experimental and homogenized results of specimens printed in *XY* and *XZ* directions. From the table, it is evident that the elastic modulus increases with the addition of fiber content for FGM, and CF/ABS specimens fabricated on the *XY* plane. The trend is not as consistent as other directions for both homogenized and experimental samples. The overall results of the numerical method showed the maximum error of less than 14% in comparison with the experimental test results. The prediction of Young's moduli is accurate for neat ABS, CF/ABS, and FGM samples fabricated on the *XY* plane. However, the error percentage increases for the specimens printed on the *XZ* plane. An acceptable range is between 10 and 14 % for ABS and FGM materials. However, Young's modulus yielded reasonable results for the CF/ABS manufactured on the *XZ* plane. The approximate fiber orientation and length distribution were obtained from the

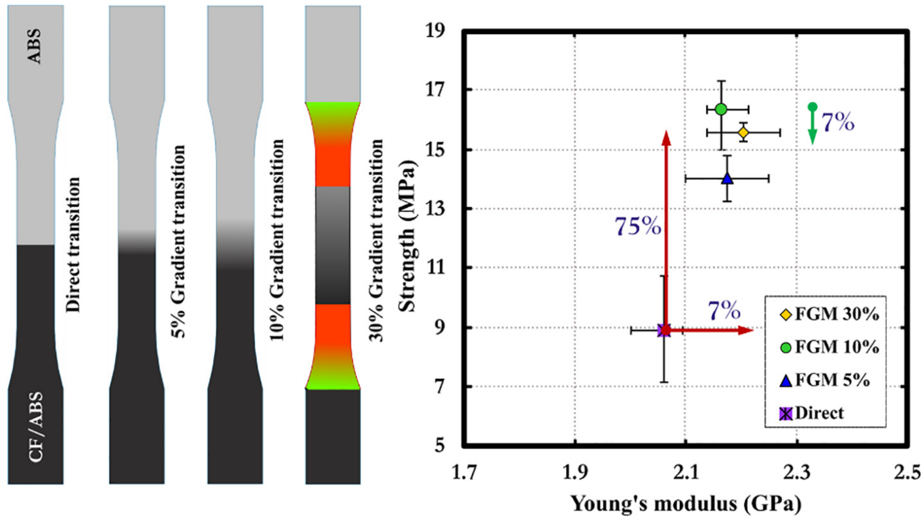

Fig. 12. Comparison of FGM designs with respect to the direct transition.

Table 2
Comparison of experimental and homogenized results obtained for neat ABS, FGM, and CF/ABS for *XY* and *XZ* orientations.

	Young's Moduli (GPa)		Error %
	Experimental test results	Homogenized values	
ABS XY	2.291 ± 0.025	2.256	1.53
ABS *XZ*	2.261 ± 0.425	2.019	11.99
CF/ABS XY	4.911 ± 0.052	4.958	0.96
CF/ABS *XZ*	2.701 ± 0.083	2.659	1.55
FGM XY	3.256 ± 0.067	3.399	4.39
FGM *XZ*	1.987 ± 0.032	2.249	13.18

microstructural description, and fiber–matrix interface was assumed to be perfect. These assumptions could have increased the errors between the predicted and experimentally tested specimens.

The homogenized results for the ABS and FGM specimens fabricated in the *XZ* direction have higher relative errors than *XY* specimens. One possible reason for high errors in the vertical direction is poor layer-to-layer adhesion quality of the fabricated specimens. Since periodic voids occur between the layer and bead, the strength of the interface between layers depends on the affinity of the layers. In this case, the joint region becomes dependent on the proper interface bond and the size of contact area between the layers. The phenomenon as presented in Fig. 13 shows the staircase shape of the outer surface of the specimen. Staircase shapes act as stress concentrators at the outer surface of the specimen that are prone to have a crack-initiation area. These staircase effects contribute more to the weakness of the specimen and create delamination between layers where the load acts transversely to the printing direction.

Specimens fabricated on the *XY* plane (printing direction) yielded the highest strength and modulus values when they are tested along the 0 or 90 layups orientations. It can be concluded that CF/ABS specimens produced better tensile strength and modulus properties than the other materials because the fibers were mainly oriented in the printing direction. It is important to clarify that the bond strength between dissimilar materials is hard to achieve. This often results in structural weakness, which is vulnerable to delamination. Fig. 14 shows the normal stress distribution at the interface of different tensile specimens tested on the *XZ* orientation to validate the experimental test results reported in Fig. 11. The direct interface pattern shows the highest stress concentration at the joint region of the ABS and CF/ABS materials. The lowest tensile strength recorded is due to the sharp transition between materials and material properties.

A gradual transition between materials however reduces the stress concentration regions. Fig. 14(a), (b), (c) indicate that the longer the linear transition length, the fewer stress concentrators acting at the interface, which eventually increase the bonding quality of constituent materials. Due to the nature of the ASTM D638 tensile test specimen geometry, stress concentrations act at the starting location of gauge area which may add extra weakness on FGM 30% and 100% transition specimens (Fig. 14(d), (e)).

Fig. 15 shows the comparison of predicted stiffness of interface patterns with the experimental test results. The error percentage between FGM 100% and the experimental result was higher than other specimens. Predicted and experimental results showed less than 7% relative error values. The graphs indicates that the homogenization framework is congruent with the experimental results, making it is an effective method to predict material properties of 3D printed parts.

3.5. Analysis of concentrations of ABS and CF/ABS materials

Homogenization of a mesoscale RVE was modeled and the macroscale material property of the heterogeneous material was predicted. Volume fractions of both ABS and CF/ABS materials were fabricated using a multi-material dual filament single extruder to analyze and understand the behavior of material properties for each concentration. Fig. 16 shows the variation of material properties of neat ABS and CF/ABS materials. It is known that the increase in fiber concentration in matrix materials improves the material properties of the fabricated components. A similar scenario is valid here as well, and the difference is only the processing condition (functionally graded AM). The multimaterial printing capability allows the fiber concertation to be varied within the model geometry. The increase of the CF/ABS concentration results in the increase in stiffness properties from *neat* ABS to a CF/ABS composite filament. The goal of fabricating different volume fractions of the constituent materials (ranging from 20% to 80 % by volume) is to understand the behavior of the blended material property at a specific location of the FGM sample.

Tensile test results in Fig. 17 reveal the variation of material properties from *neat* ABS to CF/ABS. The graph shows the linear trend from *neat* to SCF reinforced ABS materials fabricated on the *XY* plane. Since the bonding strength heavily depends on the layer-to-layer adhesion and the surface quality of the specimens, the *XZ*-oriented specimen does not follow the appropriate trend. The tensile strength and stiff-

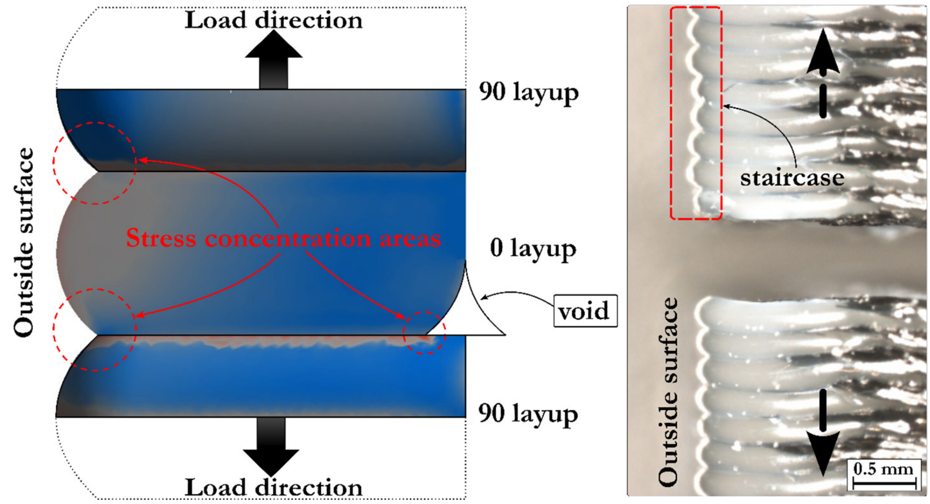

Fig. 13. Mesostructure of the vertical printed sample (*XZ*) showing stress concentration areas on the left and optical microscopical image of the fractured specimen on the right.

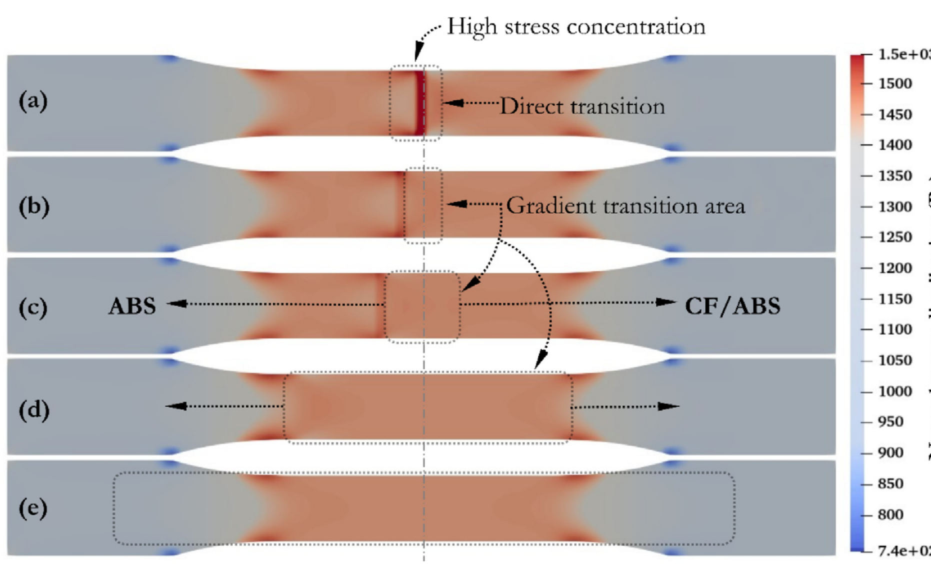

Fig. 14. Normal stress distribution at the interface of the tensile samples, (a) direct transition from ABS to CF/ABS, (b) gradient transition within 5% of total length, (c) gradient transition within 10% of total length, (d) gradient transition within 30% of total length, (e) 100% linear transition throughout the specimen.

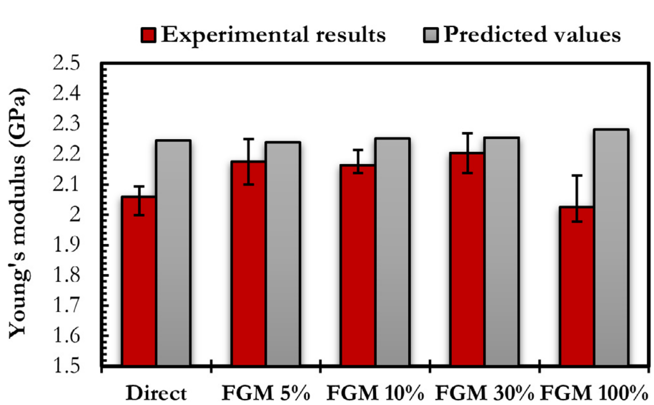

Fig. 15. Comparison of predicted Young's moduli of interface patterns in comparison with experimental test results.

ness of *XZ* samples are in the range of 22–30 MPa. According to the microstructural measurements and assumptions made on determining the fiber orientation and length distribution, the fibers were mainly oriented in 0 and 90 directions. In these directions, the fibers significantly contribute to the strength of the final part. However, there could be a minor effect on the mechanical properties of ABS and CF/ABS blends fabricated on the *XZ* plane. This is because the load is applied transversely to the fiber direction and did not influence the mechanical properties of 3D printed parts. As a result, there is a minor effect on the mechanical properties of ABS and CF/ABS blends fabricated on the *XZ* plane. Fibers only act as a stress concentrator inside the ABS matrix during tensile testing and do not contribute immensely to the strength of *XZ* specimens.

Fiber reinforcements affect the toughness of the material blends as well and indicate a decreasing trend as shown in Fig. 17.

Homogenization of a mesoscale RVE was modeled, and the macroscale material property of the heterogeneous material was predicted.

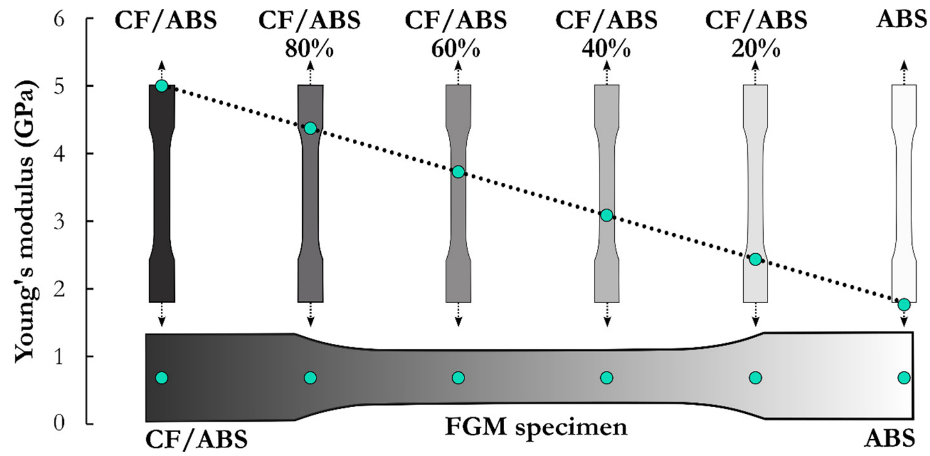

Fig. 16. Graphical representations of concentrations of ABS and CF/ABS materials fabricated to test mechanical behavior of heterogeneous blends and provide understanding of the gradual change of Young's modulus at specific locations on the FGM specimen (arrows show the loading directions).

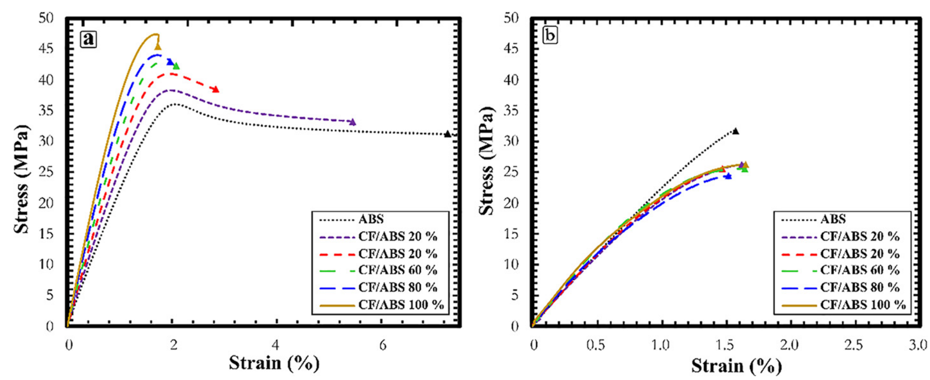

Fig. 17. Stress and strain graph of neat ABS and CF/ABS with varying concentrations (by volume %) of each filament, (a) specimen printed on XY plane, (b) specimen printed on XZ plane.

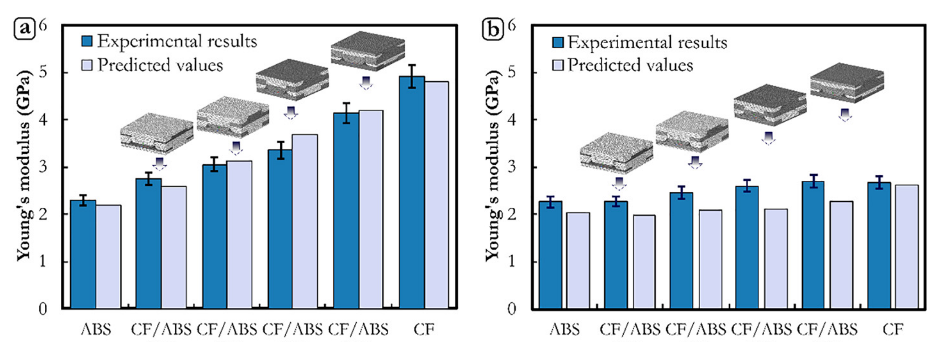

Fig. 18. Comparison of experimental and predicted FGM specimens showing various volume fractions of ABS and CF/ABS materials, (a) specimens fabricated on XY plane, (b) specimens fabricated on XZ plane.

The comparison of predicted material properties of volume concentrations of ABS and CF/ABS materials was presented in Fig. 18. Results predicted by *XY* and experimental results showed less than 10% error, and predicted material properties followed the increasing trend from ABS to CF/ABS. Since the CF/ABS composite phase increases its volume fraction (SCF concentration increases as well) in the bead (Fig. 9), the Young's modulus of material blends also increases from neat ABS to a CF/ABS composite.

Fig. 19 shows that the SCF inside the ABS matrix is mainly aligned with the printing direction. As the tensile load is applied transversely, fibers act as the stress concentrators, resulting in the formation of local stresses and these stresses initiate cracks that propagate at the interface of two materials and result in matrix cracking. Although the fibers always act as a stress concentrators, there is a substantial contribution of fiber orientation on the mechanical properties of the final component.

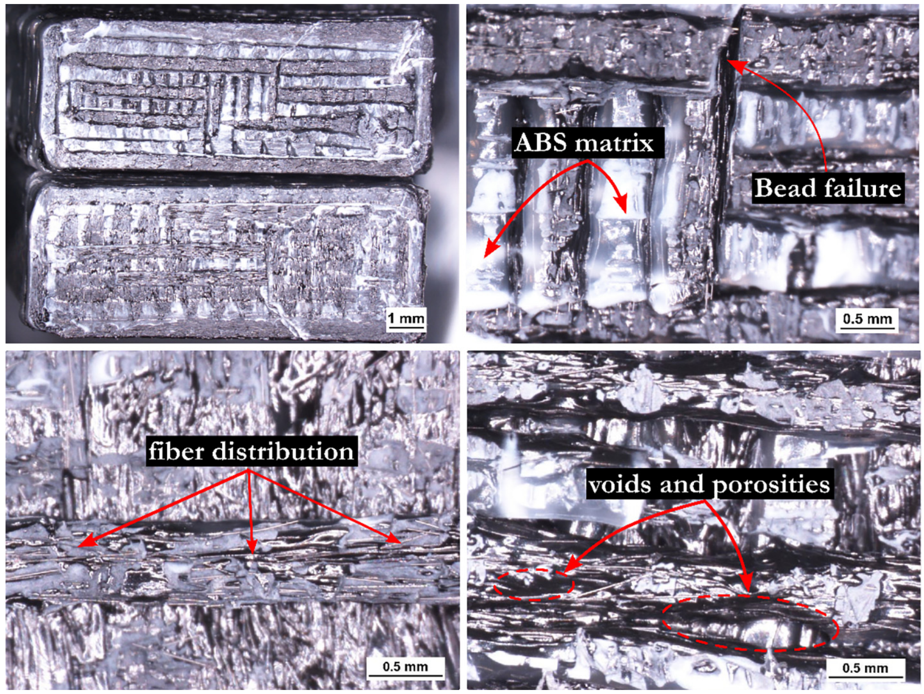

Fig. 19. Micrography of FGM specimen fabricated and tested on *XZ* plane.

4. Conclusion

To conclude, this study presented the modeling of FGM composites using a three-scale homogenization framework and investigated material transition strength using the tensile test method. The effective material properties predicted by the homogenization framework for *XY* blended samples confirm the validity of the experimental test methods. Fiber orientations, length distributions, and fiber volume fractions in the ABS matrixes were determined using microscopical images and TGA analysis.

The main findings of the study are:

- Approximate fiber orientation and distribution were determined using microscopic images. These were successfully used to estimate the fiber orientation tensor to perform the microscale homogenization process.
- Relative errors in the prediction of Young's moduli for ABS, FGM, and CF/ABS composites were less than 5% for the *XY* specimen, however, the *XZ* specimen showed higher error values ($^{\text{approximately}}$ 14%) than the *XY* counterpart due to poor layer-to-layer adhesion and surface roughness.
- The FGM specimen fabricated on the *XY* plane yielded higher strength and stiffness properties than *neat* ABS material due to the addition of a fiber reinforcement and aligned fiber orientations. Although the tensile strength of FGM was lower than *neat* ABS for *XZ* oriented specimens, the FGM showed a higher stiffness result.
- Interface patterns were successfully designed to investigate the effect of various gradient transitions with respect to sharp transition pattern. It was concluded that the higher the transition length, the fewer the stress concentrations at the material interface region, which eventually improved the bonding strength.
- Various samples with different concentrations of ABS and CF/ABS materials were manufactured to investigate the material transition behavior and predict heterogeneous FGM material properties. Experimental results showed a linear trend, with tensile strength and stiffness property increasing from the ABS to the CF/ABS composite material for the *XY* orientation. However, this trend was not consistent for the *XZ*-fabricated specimens. Homogenized values were congruent with the experimental results for both *XY* and *XZ* oriented samples.

It is envisaged that experimental data from this study will lead to optimally designed composite FGMs at less cost, reduced weight, and enhanced performance. Future work will include the optimization of material distribution along with the gradient material transition zone. Since fiber length and angle distribution were defined based on approximations, computed tomography could be employed as an experimental technique to measure fiber orientation and length distribution for more accurate results. Finally, microscale could include porosities and voids that can be characterized and included in microscale-generation algorithms.

Declaration of Competing Interest

The authors declare that they have no known competing financial interests or personal relationships that could have appeared to influence the work reported in this paper.

Acknowledgements

This study has been performed at the Additive Manufacturing Research and Innovation Laboratory of Tennessee Tech University. Technical and professional support provided by Amy Hill and Aslan Nasirov is appreciated. The research assistantship support provided by NSF Award 1601587, AM-WATCH: Additive Manufacturing – Workforce Advancement Training Coalition and Hub, is also greatly appreciated.

References

[1] Wohlers TT, Campbell I. (Specialist in three dimensional printing), Diegel O, Kowen J. Wohlers report 2018 : 3D printing and additive manufacturing state of the industry : annual worldwide progress report. n.d.

[2] Fidan I, Imeri A, Gupta A, Hasanov S, Nasirov A, Elliott A, et al. The trends and challenges of fiber reinforced additive manufacturing. Int J Adv Manuf Technol 2019;102(5-8):1801–18. https://doi.org/10.1007/s00170-018-03269-7.

[3] Gupta A, Hasanov S, Fidan I. Processing and characterization of 3d-printed polymer matrix composites reinforced with discontinuous fibers. Proc 30th Annu Int Solid Free Fabr Symp – An Addit Manuf Conf 2019:1054–66.
[4] Brackett J, Yan Y, Cauthen D, Kishore V, Lindahl J. Development of functionally graded material capabilities in large-scale extrusion deposition additive manufacturing. Proc 30th Annu Int Solid Free Fabr Symp – An Addit Manuf Conf 2019:1793–803.
[5] Hasanov S, Gupta A, Nasirov A, Fidan I. Mechanical characterization of functionally graded materials produced by the fused filament fabrication process. J Manuf Process 2020;58:923–35. https://doi.org/10.1016/j.jmapro.2020.09.011.
[6] Lumpe TS, Mueller J, Shea K. Tensile properties of multi-material interfaces in 3D printed parts. Mater Des 2019;162:1–9. https://doi.org/10.1016/j.matdes.2018.11.024.
[7] Udupa G, Rao SS, Gangadharan KV. Functionally graded composite materials: an overview. Procedia Mater Sci 2014;5:1291–9. https://doi.org/10.1016/j.mspro.2014.07.442.
[8] Li Y, Feng Z, Hao L, Huang L, Xin C, Wang Y, et al. A review on functionally graded materials and structures via additive manufacturing: from multi-scale design to versatile functional properties. Adv Mater Technol 2020;5(6):1900981. https://doi.org/10.1002/admt.v5.610.1002/admt.201900981.
[9] Ahankari SS, Kar KK. Functionally graded composites: Processing and applications. Compos. Mater. Process. Appl. Charact., Springer Berlin Heidelberg; 2016, p. 119–68. https://doi.org/10.1007/978-3-662-49514-8_4.
[10] Kieback B, Neubrand A, Riedel H. Processing techniques for functionally graded materials. Mater Sci Eng A 2003;362(1-2):81–106. https://doi.org/10.1016/S0921-5093(03)00578-1.
[11] Chung H, Das S. Processing and properties of glass bead particulate-filled functionally graded Nylon-11 composites produced by selective laser sintering. Mater Sci Eng A 2006;437(2):226–34. https://doi.org/10.1016/j.msea.2006.07.112.
[12] Hofmann DC, Roberts S, Otis R, Kolodziejska J, Dillon RP, Suh J-O, et al. Developing gradient metal alloys through radial deposition additive manufacturing. Sci Rep 2015;4(1). https://doi.org/10.1038/srep05357.
[13] Ituarte IF, Boddeti N, Hassani V, Dunn ML, Rosen DW. Design and additive manufacture of functionally graded structures based on digital materials. Addit Manuf 2019;30:100839. https://doi.org/10.1016/j.addma.2019.100839.
[14] Ning F, Cong W, Hu Y, Wang H. Additive manufacturing of carbon fiber-reinforced plastic composites using fused deposition modeling: Effects of process parameters on tensile properties. J Compos Mater 2017;51(4):451–62. https://doi.org/10.1177/0021998316646169.
[15] Mohammadizadeh M, Imeri A, Fidan I, Elkelany M. 3D printed fiber reinforced polymer composites – Structural analysis. Compos Part B Eng 2019;175:107112. https://doi.org/10.1016/j.compositesb.2019.107112.
[16] Hofstätter T, Pedersen DB, Tosello G, Hansen HN. State-of-the-art of fiber-reinforced polymers in additive manufacturing technologies. J Reinf Plast Compos 2017;36(15):1061–73. https://doi.org/10.1177/0731684417695648.
[17] Nasirov A, Gupta A, Hasanov S, Fidan I. Three-scale asymptotic homogenization of short fiber reinforced additively manufactured polymer composites. Compos Part B Eng 2020;202:108269. https://doi.org/10.1016/j.compositesb.2020.108269.
[18] Li DH, Wan AS. A layerwise multiscale analysis method for composite laminated plates. Compos Struct 2021;257:113157. https://doi.org/10.1016/j.compstruct.2020.113157.
[19] Aluko O, Gowtham S, Odegard GM. The development of multiscale models for predicting the mechanical response of GNP reinforced composite plate. Compos Struct 2018;206:526–34. https://doi.org/10.1016/j.compstruct.2018.08.093.
[20] Raju B, Hiremath SR, Roy MD. A review of micromechanics based models for effective elastic properties of reinforced polymer matrix composites. Compos Struct 2018;204:607–19. https://doi.org/10.1016/j.compstruct.2018.07.125.
[21] Guo Q, Yao W, Li W, Gupta N. Constitutive models for the structural analysis of composite materials for the finite element analysis: a review of recent practices. Compos Struct 2021;260:113267. https://doi.org/10.1016/j.compstruct.2020.113267.
[22] Torrado AR, Shemelya CM, English JD, Lin Y, Wicker RB, Roberson DA. Characterizing the effect of additives to ABS on the mechanical property anisotropy of specimens fabricated by material extrusion 3D printing. Addit Manuf 2015;6:16–29. https://doi.org/10.1016/j.addma.2015.02.001.
[23] Nasirov A, Fidan I. Prediction of mechanical properties of fused filament fabricated structures via asymptotic homogenization. Mech Mater 2020;145:103372. https://doi.org/10.1016/j.mechmat.2020.103372.
[24] Pei S, Wang K, Chen C-B, Li J, Li Y, Zeng D, et al. Process-structure-property analysis of short carbon fiber reinforced polymer composite via fused filament fabrication. J Manuf Process 2021;64:544–56. https://doi.org/10.1016/j.jmapro.2021.02.019.
[25] Gupta A, Fidan I, Hasanov S, Nasirov A. Processing, mechanical characterization, and micrography of 3D-printed short carbon fiber reinforced polycarbonate polymer matrix composite material. Int J Adv Manuf Technol 2020;107(7-8):3185–205. https://doi.org/10.1007/s00170-020-05195-z.
[26] Liu X, Shapiro V. Homogenization of material properties in additively manufactured structures. CAD Comput Aided Des 2016;78:71–82. https://doi.org/10.1016/j.cad.2016.05.017.
[27] Nasirov A, Hasanov S, Fidan I, Technology E. Prediction of mechanical properties of fused deposition modeling made parts using multiscale modeling and classical laminate theory. Proc 30th Annu Int Solid Free Fabr Symp – An Addit Manuf Conf 2019:1373–82.
[28] Somireddy M, Czekanski A. Computational modeling of constitutive behaviour of 3D printed composite structures. J Mater Res Technol 2021;11:1710–8. https://doi.org/10.1016/j.jmrt.2021.02.030.
[29] Somireddy M, Czekanski A. Mechanical characterization of additively manufactured parts by FE modeling of mesostructure. J Manuf Mater Process 2017;1:18. https://doi.org/10.3390/jmmp1020018.
[30] Nasirov A, Hasanov S, Nasirov A, Hasanov S, Fidan I. Prediction of Mechanical Properties of Fused Deposition Modeling Made Parts using Multiscale Modeling and Classical Laminate Theory Fiber Reinforced Additive Manufacturing View project Multi material printing View project Prediction of Mechanical Properties of Fused Deposition Modeling Made Parts using Multiscale Modeling and Classical Laminate Theory. 2019.
[31] Babu KP, Mohite PM, Upadhyay CS. Development of an RVE and its stiffness predictions based on mathematical homogenization theory for short fibre composites. Int J Solids Struct 2018;130–131:80–104. https://doi.org/10.1016/j.ijsolstr.2017.10.011.
[32] Belhouideg S. Prediction of effective mechanical properties of composite materials using homogenization approach: Application to tungsten fiber reinforced bulk metallic glass matrix composite. Eur Mech Sci 2018;2:68–75. , https://doi.org/10.26701/ems.376369.
[33] Cuan-Urquizo E, Barocio E, Tejada-Ortigoza V, Pipes RB, Rodriguez CA, Roman-Flores A. Characterization of the mechanical properties of FFF structures and materials: A review on the experimental, computational and theoretical approaches. Materials (Basel) 2019;16. https://doi.org/10.3390/ma12060895.
[34] El Moumen A, Tarfaoui M, Lafdi K. Additive manufacturing of polymer composites: processing and modeling approaches. Compos Part B Eng 2019;171:166–82. https://doi.org/10.1016/j.compositesb.2019.04.029.
[35] Smith ZW and DE. Rheology Effects on Predicted Fiber Orientation and Elastic Properties in Large Scale Polymer Composite Additive Manufacturing. J Compos Sci 2018;2:10. https://doi.org/10.3390/jcs2010010.
[36] Lopes LR, Silva AF, Carneiro OS. Multi-material 3D printing: The relevance of materials affinity on the boundary interface performance. Addit Manuf 2018;23:45–52. https://doi.org/10.1016/j.addma.2018.06.027.
[37] Brackett James, Yan Yongzhe, Cauthen Dakota, Kishore Vidya, Lindahl John, Smith Tyler, et al. Characterizing material transitions in large-scale Additive Manufacturing. Addit Manuf 2021;38:101750. https://doi.org/10.1016/j.addma.2020.101750.
[38] Vu IQ, Bass LB, Williams CB, Dillard DA. Characterizing the effect of print orientation on interface integrity of multi-material jetting additive manufacturing. Addit Manuf 2018;22:447–61. https://doi.org/10.1016/j.addma.2018.05.036.
[39] Voxelizer 2 n.d. https://voxelizer.com/ (accessed May 12, 2021).
[40] Kaweesa DV, Meisel NA. Material property changes in custom-designed digital composite structures due to voxel size. Proc 29th Annu Int Solid Free Fabr Symp – An Addit Manuf Conf 2018:1499–510.
[41] Doubrovski EL, Tsai EY, Dikovsky D, Geraedts JMP, Herr H, Oxman N. Voxel-based fabrication through material property mapping: A design method for bitmap printing. CAD Comput Aided Des 2015;60:3–13. https://doi.org/10.1016/j.cad.2014.05.010.
[42] Mohammadizadeh Mahdi, Lu Hao, Fidan Ismail, Tantawi Khalid, Gupta Ankit, Hasanov Seymur, et al. Mechanical and thermal analyses of metal-PLA components fabricated by metal material extrusion. Inventions 2020;5(3):44. https://doi.org/10.3390/inventions5030044.
[43] ASTM D638 - 14 Standard Test Method for Tensile Properties of Plastics n.d. https://www.astm.org/Standards/D638.htm (accessed August 8, 2020).
[44] Hollister SJ, Kikuchi N. A comparison of homogenization and standard mechanics analyses for periodic porous composites. Comput Mech 1992;10(2):73–95. https://doi.org/10.1007/BF00369853.
[45] Material Designer Users Guide 2020:71–5.
[46] Sias DF, Oliveira BF, Maghous S, Creus GJ. Application of homogenization theory to composite materials. Jornadas Sul-Americanas Eng Estrutural Appl 2002.
[47] Somireddy M, Czekanski A, Singh CV. Development of constitutive material model of 3D printed structure via FDM. Mater Today Commun 2018;15:143–52. https://doi.org/10.1016/j.mtcomm.2018.03.004.
[48] Fallon Jacob J, McKnight Steven H, Bortner Michael J. Highly loaded fiber filled polymers for material extrusion: A review of current understanding. Addit Manuf 2019;30:100810. https://doi.org/10.1016/j.addma.2019.100810.
[49] Tang Haibin, Chen Hui, Sun Qingping, Chen Zhangxing, Yan Wentao. Experimental and computational analysis of structure-property relationship in carbon fiber reinforced polymer composites fabricated by selective laser sintering. Compos Part B Eng 2021;204:108499. https://doi.org/10.1016/j.compositesb.2020.108499.
[50] Schindelin Johannes, Rueden Curtis T, Hiner Mark C, Eliceiri Kevin W. The ImageJ ecosystem: An open platform for biomedical image analysis. Mol Reprod Dev 2015;82(7-8):518–29. https://doi.org/10.1002/mrd.22489.
[51] Kim JH, Paulino GH. Isoparametric graded finite elements for nonhomogeneous isotropic and orthotropic materials. J Appl Mech Trans ASME 2002;69:502–14. https://doi.org/10.1115/1.1467094.
[52] Dalaq AS, Abueidda DW, Abu Al-Rub RK, Jasiuk IM. Finite element prediction of effective elastic properties of interpenetrating phase composites with architectured 3D sheet reinforcements. Int J Solids Struct 2016;83:169–82. https://doi.org/10.1016/j.ijsolstr.2016.01.011.
[53] Sun Q, Rizvi GM, Bellehumeur CT, Gu P. Effect of processing conditions on the bonding quality of FDM polymer filaments. Rapid Prototyp J 2008;14(2):72–80. https://doi.org/10.1108/13552540810862028.